Electron-nuclear double-resonance analysis of diatomic sulfur and selenium defects in NaBr and NaI

S. Van Doorslaer, F. Callens, F. Maes, and E. Boesman
Laboratory for Crystallography and Study of the Solid State, Krijgslaan 281-S1, B-9000 Gent, Belgium
(Received 12 January 1996; revised manuscript received 14 March 1996)

In this work, a single-crystal electron-nuclear double-resonance (ENDOR) study of NaBr:S_2^-, NaI:S_2^-, and NaBr:Se_2^- is presented. These defects have in common that the paramagnetic p lobes are parallel to the [001] axis. For all cases, the angular variation of two sets of ^{23}Na and one set of halide ENDOR transitions is investigated. The corresponding superhyperfine (SHF) and nuclear-quadrupole coupling tensors are determined. The two sodium interactions can be explained in terms of the nearest-neighboring Na^+ ions. The halide interaction is caused by eight next-nearest-neighboring halide ions. The ENDOR results can only be explained in terms of a monovacancy model in which X_2^- (X=S, Se) ion is replacing a single halide ion on a lattice site. The nearest-neighboring Na^+ ions are found to be displaced outwards. The linewidth of the EPR signals can be simulated using the ENDOR SHF data. [S0163-1829(96)06326-6]

I. INTRODUCTION

Although diatomic chalcogen ions in alkali halides were extensively studied in the past using EPR,[1–12] luminescence[13] and Raman[14] techniques, a lot of questions remained unanswered. It could not unambiguously be determined how the X_2^- ions (X=O, S, Se) are built into the alkali-halide lattice. Two models were suggested:[8,9] the monovacancy model, in which the X_2^- ion is replacing a single halide ion on a lattice site and a divacancy model, where the defect ion is replacing two adjacent halide ions. Furthermore, the paramagnetic lobes of the X_2^- ion were found to be pointing either along the [001] axis, either along the $[\bar{1}10]$ axis. The occurrence of both situations could not be explained. In order to solve these problems, electron-nuclear double-resonance (ENDOR) studies on a series of X_2^- defects were started. The ENDOR investigations of O_2^- in RbCl (Ref. 15) and RbI,[16] and S_2^- in RbCl (Ref. 17) and RbI (Ref. 18) were already reported. These defects have in common that the paramagnetic X_2^- p lobes are pointing along the $[\bar{1}10]$ axis. In this article, an ENDOR study of S_2^- in NaBr and NaI and of Se_2^- in NaBr is presented. The paramagnetic lobes of these ions are parallel to the [001] axis. Consequently, this ENDOR analysis is clearly distinct from the ones performed earlier.[15–18]

TABLE I. The EPR and ENDOR detection conditions for NaBr:S_2^-, NaBr:Se_2 and NaI:S_2^-.

	EPR detection conditions		ENDOR detection conditions		
	T (K)	Microwave power (mW)	T (K)	Microwave power (mW)	Modulation depth (kHz)
NaBr:S_2^-	30	1	7.0	100	100
NaI:S_2^-	4–20	1	7.0	20	100
NaBr:Se_2^-	30	200	7.5	100	140

II. EXPERIMENTAL TECHNIQUES

The single crystals were grown by the Bridgman method. The crystals were x-ray irradiated at room temperature for typically 1/2 h with a tungsten anticathode Philips x-ray tube, operated at 60 kV and 40 mA.

The EPR and ENDOR spectra were measured using the Bruker equipment described in earlier work.[15–18] In Table I, the best EPR and ENDOR detection conditions are shown.

III. RESULTS AND DISCUSSION

A. EPR results

NaBr:S_2^-,[10] NaI:S_2^-,[4] and NaBr:Se_2^- (Ref. 11) were investigated earlier using EPR. Table II shows the principal values of the orthorombic-I g tensor of these defects.

B. ENDOR results

The ENDOR angular variations were measured in the g_x-g_z plane ($B_0 \perp [001]$, plane 1) and a plane that contains the g_y axis ($B_0 \perp [100]$ or $B_0 \perp [010]$, plane 2). For all defects, one halide and two sodium interactions could be resolved. The ENDOR frequencies were analyzed through complete diagonalization of the spin-Hamiltonian matrix.

For NaBr:S_2^-, NaBr:Se_2^-, and NaI:S_2^- a complete angular variation of one set of halide (^{79}Br and ^{81}Br or ^{127}I) interactions was found. All halide interactions are characterized by a triclinic superhyperfine (SHF) and nuclear quadrupole tensor. The principal values and corresponding axes are given in Tables III and IV, respectively. Figure 1 shows for NaI:S_2^-

TABLE II. The principal values of the orthorhombic-I g tensor for NaBr:S_2^- (Ref. 10), NaBr:Se_2^- (Ref. 11), and NaI:S_2^- (Ref. 4).

	g_x ($[\bar{1}10]$)	g_y ([001])	g_z ([110])
NaBr:S_2^-	2.0114	1.9876	2.2376
NaI:S_2^-	2.0178	1.9942	2.2303
NaBr:Se_2^-	1.9007	1.8079	2.8073

TABLE III. The principal values (in MHz) and axes of the ^{79}Br and ^{81}Br superhyperfine and nuclear-quadrupole tensors of the halide interaction of NaBr:S_2^- and NaBr:Se_2^-.

NaBr:S_2^-			Angles with respect to		
	^{79}Br	^{81}Br	g_x	g_y	g_z
A_x	22.47	24.22	135.0	49.0	74.6
A_y	8.44	9.10	122.4	137.8	66.0
A_z	8.24	8.87	62.4	81.7	29.0
Q_x	−1.62	−1.38	121.8	36.7	73.6
Q_y	1.39	1.18	52.5	54.0	122.2
Q_z	0.23	0.20	126.4	96.2	142.9
NaBr:Se_2^-			Angles with respect to		
	^{79}Br	^{81}Br	g_x	g_y	g_z
A_x	31.99	34.49	148.0	61.3	77.1
A_y	10.46	11.27	67.8	32.4	112.3
A_z	9.35	10.08	111.7	103.8	153.9
Q_x	−2.31	−1.95	134.3	51.8	68.9
Q_y	1.96	1.66	63.0	39.4	116.4
Q_z	0.35	0.29	123.6	98.5	145.1

an example of the experimental angular variations. The theoretical angular variations, calculated using Table IV are shown in Fig. 1 (full lines).

In the ENDOR spectra of NaBr:S_2^-, NaBr:Se_2^-, and NaI:S_2^-, transitions belonging to two ^{23}Na interactions were also found. Interaction 1 is characterized by a monoclinic-II SHF and nuclear quadrupole tensor. The corresponding A and Q tensors are given in Table V. Figure 2 shows the observed angular variation for NaBr:S_2^-. Analogous angular variations were measured for the other defects. Sodium interaction 2 is in all cases characterized by an orthorhombic-I A and Q tensor. The principal values of these tensors are given in Table VI. For NaBr:Se_2^-, the Q tensor could not be resolved. The sign of the principal A values will be discussed later. Figure 3 shows the experimental (rectangulars) and the theoretical (full lines) angular variation for Na^+ interaction 2 (NaI:S_2^-).

TABLE IV. The principal values (in MHz) and axes of the ^{127}I superhyperfine and nuclear-quadrupole tensors of the halide interaction of NaI:S_2^-.

		Angles with respect to		
	^{127}I	g_x	g_y	g_z
A_x	22.04	133.1	48.6	71.9
A_y	8.53	91.9	117.0	27.1
A_z	7.68	43.2	53.3	70.6
Q_x	0.63	110.9	20.9	91.3
Q_y	−0.61	50.3	76.9	137.4
Q_z	−0.02	133.0	106.1	132.6

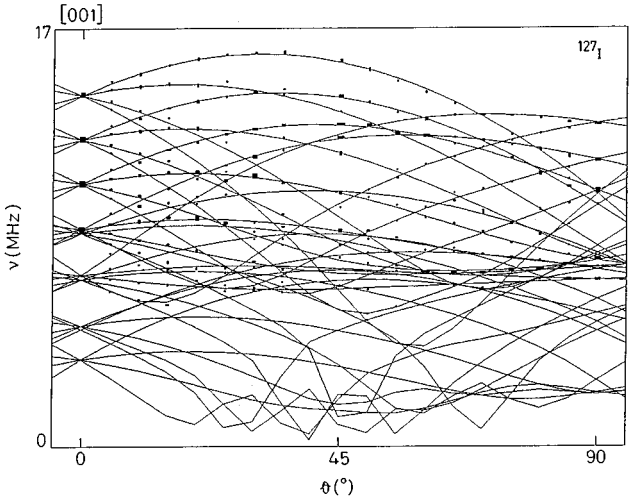

FIG. 1. ^{127}I ENDOR angular variation in plane 2 (NaI:S_2^-). Rectangles: experimental points, lines: theoretical angular variation calculated using the values of Table IV.

C. Discussion

With regard to symmetry considerations, all observed halide and sodium interactions agree with both the mono and divacancy model. In a monovacancy model, the A and Q tensors corresponding with alkali nuclei A [Fig. 4(a)] will have a monoclinic-II symmetry. This is also true for the alkali nuclei E' in the divacancy model [Fig. 4(b)]. The observed Na interactions 1 are indeed characterized by a monoclinic-II A and Q tensor (Table V) and thus are consistent with an interaction with nuclei A or E'. The orthorhombic-I symmetry of the A and Q tensors of Na interaction 2 (Table VI) is both in agreement with an interaction with alkali nuclei B (monovacancy) or alkali nuclei A' (divacancy) (Fig. 4). The triclinic halide A and Q tensors can be ascribed to the nuclei D in a monovacancy model or to nuclei G' in a divacancy model. This shows that, the model cannot be determined unambiguously from symmetry considerations alone.

For all defects, it is observed that the principal values of the sodium SHF interactions 1 and 2 are comparable in magnitude (Tables V and VI). Since, in a monovacancy model nuclei A and B are at the same distance from the center of

TABLE V. The principal values (in MHz) of the monoclinic-II A and Q tensors for Na interaction 1 of NaBr:S_2^-, NaBr:Se_2^-, and NaI:S_2^-. The tilt angles α_1 (α_2) between the A_x (Q_x) axis and the g_x axis are mentioned.

	NaBr:S_2^-	NaI:S_2^-	NaBr:Se_2^-
A_x ($[\bar{1}10]+\alpha_1$)	3.96	3.40	5.76
A_y ([001])	3.60	3.20	5.03
A_z ([110]+α_1)	2.90	2.39	2.40
α_1	55.5°	54.3°	7.7°
Q_x ($[\bar{1}10]+\alpha_2$)	−0.41	−0.28	−0.46
Q_y ([001])	0.17	0.12	0.21
Q_z ([110]+α_2)	0.24	0.16	0.25
α_2	−36.3°	−33.6°	−32.9°

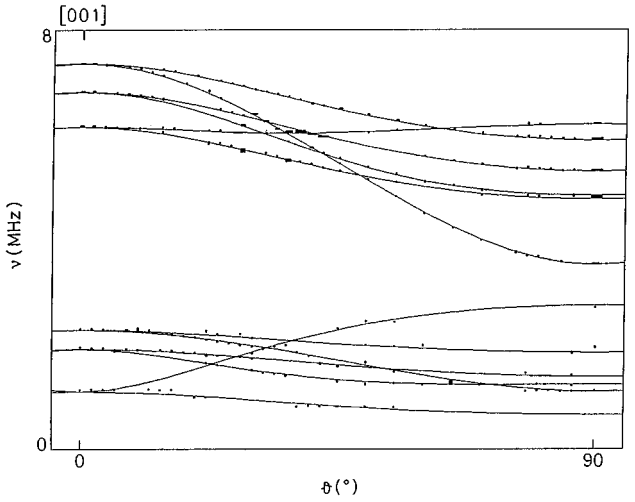

FIG. 2. ^{23}Na ENDOR angular variation in plane 2 for interaction 1 (NaBr:Se_2^-). Rectangles: experimental points, lines: theoretical angular variation calculated using the values of Table V.

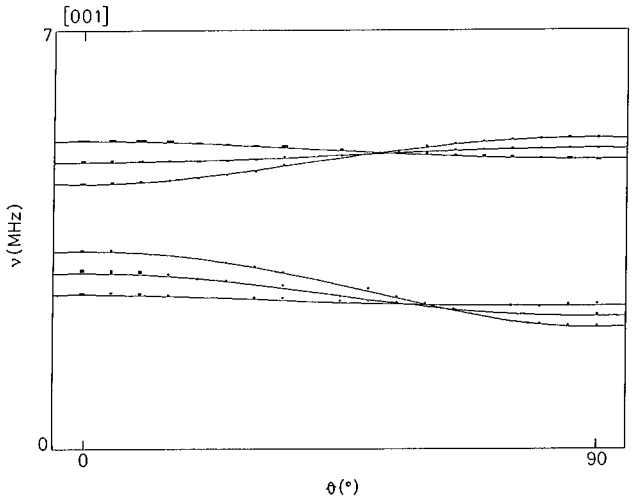

FIG. 3. ^{23}Na ENDOR angular variation in plane 2 for interaction 2 (NaI:S_2^-). Rectangles: experimental points, lines: theoretical angular variation calculated using the values of Table VI.

the chalcogen ion, we expect comparable interactions in contrast to the divacancy case. This is confirmed in the ENDOR analysis of the V_K and H center in LiF.[19–21]

Moreover, for the V_K center, an interaction with Li^+ ions C' is found (characterized by a monoclinic-I A tensor). This interaction was not recorded in the samples under investigation, although a strong interaction would be expected in view of the orientation of the paramagnetic p lobes.

The halide interactions are much stronger than the alkali interactions. This suggests a monovacancy model, because the nuclei D are much closer to the X_2^- ion than the nuclei G' (Fig. 4). In the next paragraphs, the observed interactions will be examined in detail.

1. The superhyperfine interactions

All calculations were done assuming the internuclear distance to be 0.189 nm (Ref. 23) for S_2^- and 0.215 nm (Ref. 23) for Se_2^-.

a. Halide interactions. The SHF matrix elements are large in comparison with the sodium interaction, which suggests a large overlap with the paramagnetic Γ_4^+ (p_y) lobes of the X_2^- ion. Pure dipolar contributions (0.3–0.4 MHz) cannot explain the observed SHF tensors. Covalency has to be taken into account. In a monovacancy model, the strongest covalency contribution is expected.

TABLE VI. The principal values (in MHz) of the orthorhombic-I A and Q tensors for Na interaction 2 of NaBr:S_2^-, NaBr:Se_2^-, and NaI:S_2^-. The A and Q axes are parallel to the g tensor axes.

	NaBr:S_2^-	NaI:S_2^-	NaBr:Se_2^-
A_x	−4.35	−3.11	−5.52
A_y	−3.05	−1.83	−4.51
A_z	−3.27	−2.51	−4.28
Q_x	0.01	0.07	
Q_y	−0.05	−0.12	
Q_z	0.04	0.05	

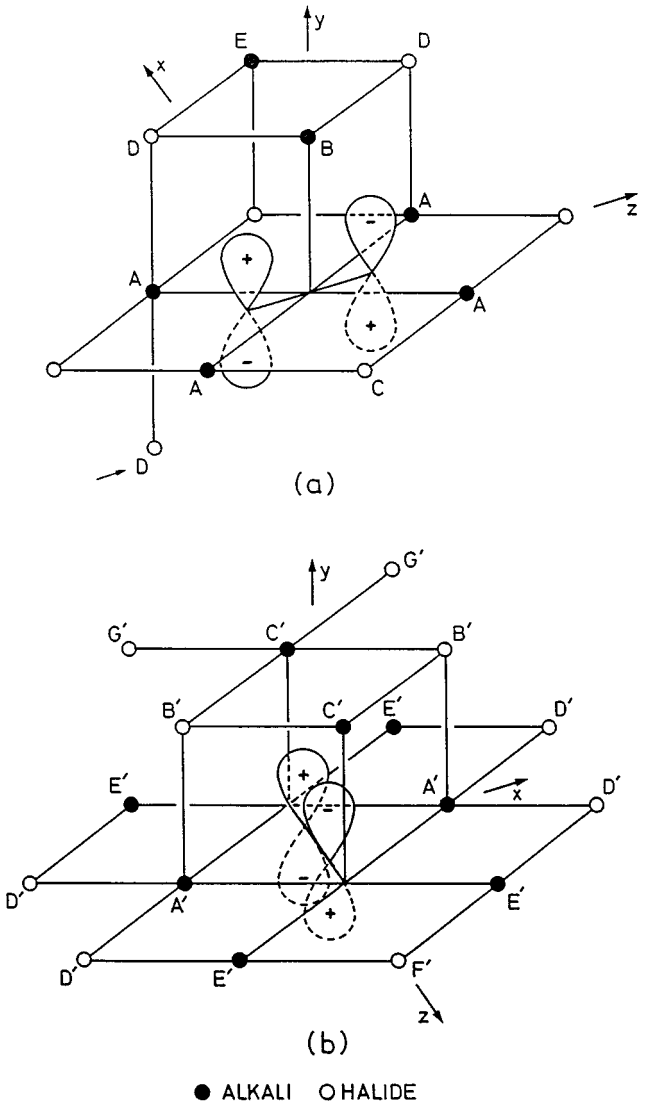

FIG. 4. (a) The monovacancy model, (b) the divacancy model.

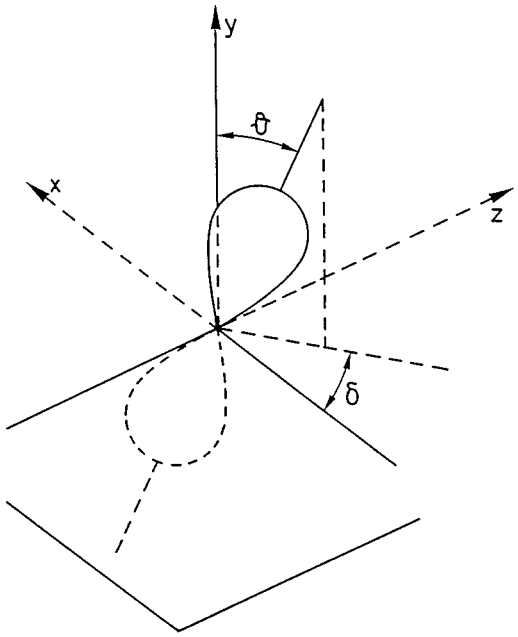

FIG. 5. θ and δ determine the orientation of the interacting halide ϕ_σ lobe for a nucleus D on a $[\bar{1}01]$ site.

The ${}^2\Gamma_4^+$ ground state of the observed X_2^- centers, can be described as follows:[2–4]

$$|\psi\pm\rangle=\cos\ \alpha|\Gamma_4^+\rangle|\pm\tfrac{1}{2}\rangle\pm i\ \sin\ \alpha|\Gamma_2^+\rangle|\pm\tfrac{1}{2}\rangle$$
$$\pm\frac{\lambda}{2E}\ (\cos\ \alpha-\sin\ \alpha)|\Gamma_1^+\rangle|\mp\tfrac{1}{2}\rangle \qquad (1)$$

with $\tan(2\alpha)=\lambda/\Delta$, $|\pm 1/2\rangle$ the eigenstates of S_z, and wherein Γ_1^+, Γ_2^+, and Γ_4^+ are irreducible representations of the D_{2h} symmetry group.[24] λ/Δ and E are defined and quantified in earlier work.[4,10,11] The p_x, p_y, and p_z lobes of the halide ions D can overlap with both the Γ_4^+ and Γ_2^+ lobes of the defect. Let us assume in a first approximation that the X_2^- defect has a pure Γ_4^+ ground state ($\sin\alpha$ is small). The wave function of the unpaired electron in the neighborhood of the halide nucleus D on a $[101]$ place (see Fig. 4, arrow) is given by

$$|\psi\rangle\approx c_\sigma\phi_\sigma+c_s\phi_s$$
$$\phi_\sigma=\cos\ \theta(np)_y+[-\cos\ \delta(np)_x+\sin\ \delta(np)_z]\sin\ \theta, \qquad (2)$$

δ and θ are defined as in Fig. 5.

The resulting contribution consists of an isotropic A_s (depending on c_s^2) and anisotropic contribution. The anisotropic contribution is

$$A_{xx}^c=[\tfrac{6}{5}\ (\cos^2\ \delta\ \sin^2\ \theta-\tfrac{1}{3})c_\sigma^2\langle r^{-3}\rangle_{\rm hal}]{\rm const},$$
$$A_{yy}^c=[(\tfrac{4}{5}\ \cos^2\ \theta-\tfrac{2}{5}\ \sin^2\ \theta)c_\sigma^2\langle r^{-3}\rangle_{\rm hal}]{\rm const},$$
$$A_{zz}^c=[\tfrac{6}{5}\ (\sin^2\ \delta\ \sin^2\ \theta-\tfrac{1}{3})c_\sigma^2\langle r^{-3}\rangle_{\rm hal}]{\rm const},$$
$$A_{xy}^c=-\tfrac{3}{5}\ \sin(2\theta)\cos\ \delta c_\sigma^2\langle r^{-3}\rangle_{\rm hal}{\rm const}=A_{yx}^c,$$
$$A_{yz}^c=\tfrac{3}{5}\ \sin(2\theta)\sin\ \delta c_\sigma^2\langle r^{-3}\rangle_{\rm hal}{\rm const}=A_{zy}^c,$$

TABLE VII. The calculated c_s^2, c_σ^2, r, θ, and δ values for the halide interactions, derived from the ENDOR data.

	c_s^2	c_σ^2	θ	δ	r	Averaged deviation
NaBr:S_2^-	0.000 63	0.008 12	49.3	19.8	0.414 nm	0.63%
NaI:S_2^-	0.000 66	0.008 20	48.9	24.1	0.448 nm	1.63%
NaBr:Se_2^-	0.000 84	0.013 03	61.8	14.3	0.414 nm	1.66%

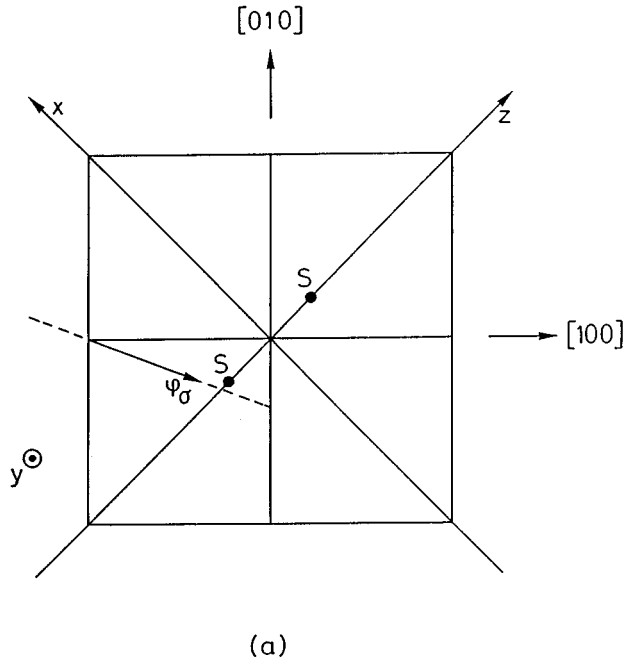

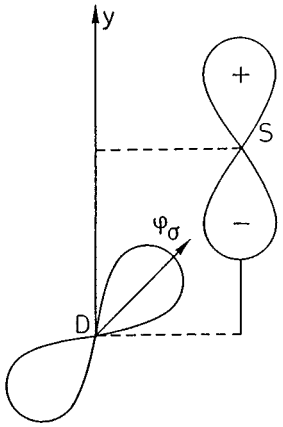

FIG. 6. Orientation of the halide ϕ_σ lobe in the NaI:S_2^- case [(a) view from above, (b) side view (section along ---- line)]. The angle between the ϕ_σ lobe and the y axis is θ (see also Fig. 5).

TABLE VIII. The values of A_s, c_σ^2, and r, derived from sodium ENDOR interaction 2 for NaBr:S_2^-, NaBr:Se_2^-, and NaI:S_2^-. $\Delta r(>0)$ is the displacement of the Na nuclei with respect to the normal lattice position. $2a$ is the lattice constant.

	A_s	c_σ^2	r	Δr
NaBr:S_2^-	−3.54 MHz	0.000 35	0.35 nm	0.19 a
NaI:S_2^-	−2.47 MHz	0.000 17	0.36 nm	0.13 a
NaBr:Se_2^-	−4.72 MHz	0.000 45	0.37 nm	0.26 a

$$A_{xz}^c = -\tfrac{3}{5}\sin(2\delta)\sin^2\theta c_\sigma^2\langle r^{-3}\rangle_{\rm hal}\text{const} = A_{zx}^c, \qquad (3)$$

with

$$\text{const} = \frac{\mu_0}{4\pi h} g_N g_e \beta\beta_N 10^{-6}. \qquad (4)$$

For $^{79}Br^-$: $\langle r^{-3}\rangle_{\rm hal}=10.22$ a.u.; for $^{127}I^-$: $\langle r^{-3}\rangle_{\rm hal}=12.73$ a.u.[25]

The dipole-dipole contribution to the A matrix was calculated taking into account the spatial distribution of the unpaired electron over the X_2^- ion. When the dipole-dipole matrix elements A_{ij}^d are added to A_s and A_{ij}^c, a asymmetrical matrix A is obtained. The symmetrical matrix $(A)^T(A)$ has to be compared with the experimental A matrices refered to the g tensor axes. In Table VII the results of this fitting are shown. The averaged deviation is the ratio of the difference between the experimental and theoretical A values versus the experimental values.

Figure 6 (based on the results of Table VII) shows that the interacting lobe points to the nearest p_y lobe of the X_2^- ion, in a way expected in a monovacancy model. In a divacancy model, δ would be expected to be approximately 60–70°. It is observed that the c_s^2 and c_σ^2 coefficients are larger for NaBr:Se_2^- than for NaBr:S_2^-. This is expected, since the larger Se_2^- ion will overlap more with the Br lobes. The c_s^2 and c_σ^2 coefficients for the S_2^- ion in NaBr and NaI are approximately the same. Indeed, although the I^--S_2^- distance is larger than the Br^--S_2^- distance, this is compensated by the larger polarizability of I^-.

b. Sodium interactions. For all studied crystals, two *sodium interactions* were observed. We first focus on interaction 2. In a monovacancy model, the only reasonable possibility that does not lower the orthorhombic-I symmetry of the A and Q tensors is that of the two nearest-neighboring Na^+ ions B along the [001] axis [Fig. 4(a)].

Since only the interaction between the Na $2p_z$ orbitals and the $X_2^-\Gamma_4^+$ orbitals is symmetry allowed, the sign of the principal A values is taken negative in agreement with earlier ENDOR studies of X_2^- defects with Γ_2^+ ground state.[15–18] The wave function of the unpaired electron in the neighborhood of the alkali nucleus is

$$|\psi\rangle \approx \cos\alpha c_\sigma (2p)_z, \qquad (5)$$

which results in the following components (in MHz) for the A^c matrix:

$$A_x^c = -\tfrac{2}{3} A_\sigma,$$

$$A_y^c = -\tfrac{2}{3} A_\sigma,$$

$$A_z^c = \tfrac{4}{3} A_\sigma, \qquad (6)$$

with

$$A_\sigma = \tfrac{3}{5}\cos^2\alpha c_\sigma^2\langle r^{-3}\rangle\left(\frac{\mu_0}{4\pi h} g_N g_e \beta\beta_N 10^{-6}\right) \qquad (7)$$

and $\langle r^{-3}\rangle=17.04$ a.u. for a Na nucleus.[25]

Furthermore, an isotropic part A_s and the dipole-dipole interaction has to be considered. When calculating the dipolar A^d matrix, the spatial distribution of the paramagnetic electron over the X_2^- lobes should be taken into account.[15–18]

Comparison of the summation of A_s, A^c, and A^d with the experimental A matrix, leads to the values for A_s, c_σ^2 and the distance between the halide ion and the X_2^- center r mentioned in Table VIII. It was found that only for a monovacancy model and when taking the A_s values negative, the theory could be fitted to the experimental values in a physically acceptable way. From Table VIII, we find that the Na ions are displaced 13 to 26 % outwards with respect to the normal lattice position. We should also take into account, the fact that the unpaired electron resides for 0.8% (S_2^- defects)

TABLE IX. For sodium interaction 1: Diagonal elements (in MHz) of the magnetic dipolar tensor and the angle β between the axis corresponding with the largest value and the g_x axis.

	A_x^d	A_y^d	A_z^d	β (°)
NaBr:S_2^-	1.588	−0.689	−0.899	28.15
NaI:S_2^-	1.293	−0.577	−0.707	30.10
NaBr:Se_2^-	1.625	−0.533	−0.995	8.73

TABLE X. For sodium interaction 1: The diagonal elements (in MHz) of the calculated SHF tensors and the diagonalization angle δ_1. The values of c_π^2 are also given.

	A_x	A_y	A_z	δ_1	A_s	c_π^2
NaBr:S_2^-	4.58	3.60	2.27	32.7	3.49	0.000 395
NaI:S_2^-	3.34	3.20	2.41	31.6	3.16	0.000 334
NaBr:Se_2^-	5.24	5.03	2.91	30.1	4.41	0.000 597

TABLE XI. Comparison between the EPR linewidths (in 10^{-4} T) obtained from the ENDOR results (a) and those obtained experimentally (b).

		ΔB (a)	ΔB (b)
NaBr:S_2^-	$B_0 \parallel [00\bar{1}]$	42.1	43.6
	$B_0 \parallel [\bar{1}10]$	42.7	46.4
	$B_0 \parallel [110]$	22.3	26.2
NaBr:Se_2^-	$B_0 \parallel [00\bar{1}]$	49.8	51.7
	$B_0 \parallel [\bar{1}10]$	75	77.6
	$B_0 \parallel [110]$	27.3	24.6
NaI:S_2^-	$B_0 \parallel [00\bar{1}]$	60	55[a]
	$B_0 \parallel [\bar{1}10]$	55.4	54
	$B_0 \parallel [110]$	35.2	33

[a]Vannotti *et al.* (Ref. 4) mention a linewidth of 8.5 mT, but this was not in agreement with our EPR measurements.

TABLE XII. For the halide interactions: the calculated principal values (in MHz) of the Q tensor due to the charge distribution on the nucleus. The angles between the Q_x axis and g tensor axes are given. They should be compared with Tables III and IV.

				Angles determining Q_x w.r.t.		
	Q_x	Q_y	Q_z	g_x	g_y	g_z
$Na^{79}Br:S_2^-$	−0.86	0.43	0.43	135.5°	49.3°	75.1°
$NaI:S_2^-$	0.76	−0.38	−0.38	126.9°	48.9°	65.9°
$Na^{79}Br:Se_2^-$	−1.38	0.69	0.69	148.7°	61.8°	77.4°

or 1.3% (Se_2^- defects) on each of the eight surrounding halide ions, was not considered. This will influence the calculated displacements. For the H center and the V_K center in LiF and NaF,[21–22] displacements of 16–30 % were observed for the nearest neighbors, which suggests a large flexibility of the alkali-halide lattices. Also, from the ENDOR data of $KCl:Ag^0$ and $NaCl:Ag^0$, Holmberg, Unruh, and Friauf[27] and Barriuso and Moreno[28] derived displacements of 10–20 % for the nearest surrounding ions. Using interaction potential and extended atomistic calculations, Bucher[29] estimated the nearest-neighboring displacements in these cases to be half the ones reported earlier.[26,27] These findings suggest that more refined theoretical studies might also lead to smaller displacements for the cases under study.

Table IX shows the dipolar tensors and corresponding diagonalization angle, for which the spatial distribution of the unpaired electron over the X_2^- lobes (X=S, Se) is taken into account. The alkali ions are located on a lattice site. Table IX indicated that here the dipolar contribution plays an important role in the SHF interaction. A clear difference between the diagonalization angle for $NaBr:Se_2^-$ and $NaBr:S_2^-$ was found, corresponding qualitatively to the experimentally observed tilt angles of the SHF tensors.

Covalency effects also have to be taken into account. In a first approximation, the wave function of the unpaired electron in the neighborhood of the Na nucleus A [Fig. 4(a)] can be taken as

$$|\psi\pm\rangle \approx \cos\ \alpha c_\pi (np)_y |\pm\tfrac{1}{2}\rangle \tag{8}$$

from which the SHF matrix can be calculated in a comparable way as before.

Moreover, an isotropic contribution due to spin polarization and/or configuration interaction should be considered. The combination of these three effects results in the SHF tensors mentioned in Table X. In a first approximation, A_s was taken to be the average of the three principal A values. Using this value of A_s and A_y, a starting value for A_π could be derived. Variation of A_s and A_π hardly led to better results. Comparison between Tables V and X shows that there is a large difference of about 20° between the experimental and theoretical tilt angles. Although the trend of the SHF principal values is comparable to the one found for the experimental A tensors, there is no quantitative match.

Possible causes for these results can be the following. First of all, a better approximation of the wave function of the unpaired electron in the neighborhood of the sodium nucleus is

$$|\psi\pm\rangle = \cos\ \alpha c_\pi (np)_y |\pm\tfrac{1}{2}\rangle \pm i\ \sin\ \alpha c_\sigma \underbrace{[-\cos\ \delta (np)_x + \sin\ \delta (np)_z]}_{\phi_\sigma} |\pm\tfrac{1}{2},\rangle \tag{9}$$

in which δ is the angle between the ϕ_σ lobe and the g_x axis. For the derivation of this wave function, the Γ_2^+ contribution to the wave function of the X_2^- defect [Eq. (1)] is also considered. Secondly, in the calculations of the dipole matrix, the Na nuclei were assumed to be on a lattice site. From the analysis of Na interaction 2, we derived that the nearest-neighboring Na^+ ions along the [001] axis are displaced. A displacement of the nearest Na^+ ions in the xz plane is also probable. Similar displacements were found in the ENDOR analysis of the H center in LiF.[21] In the analysis of the Q tensor of interaction 1, such a displacement will be shown to be probable.

The exact determination of the displacement is very difficult, if not impossible. As mentioned before, the dipolar contribution plays a considerable role in the SHF matrix (Table IX). Small displacements can have a large influence on the SHF interaction. On the whole, six parameters (the coordinates of the nucleus in the g_x-g_z plane, A_s, c_π, c_σ and δ) have to be derived from four experimental data. This problem obviously has an infinite number of solutions.

Finally, if we assume that the EPR linewidths can be ascribed to unresolved sodium and halide SHF interactions, then the EPR linewidths must be reconstructable using the ENDOR data. This can be done using the formulas derived by Iwasaki[30] as mentioned in earlier work.[15–18] If we assume the SHF line to have a homogeneous linewidth of 1.5×10^{-4} T, the EPR linewidths given in Table XI are obtained. Comparison with the experiment proves that the observed EPR linewidths are due to the detected SHF interactions. This again confirms the monovacancy model. Indeed, in a divacancy model a strong interaction with the nuclei C' [Fig. 4(b)] is expected. Since such an interaction was not found and the EPR linewidth could be simulated using the ENDOR data, this contradicts the divacancy model.

2. Nuclear quadrupole tensors

The nuclear quadrupole tensor Q is a measure of the total unbalanced charge density around the nucleus (contribution of the surrounding charges and of the charge distribution of the unpaired electron on the nucleus).[31,32] From Tables III and IV we derive that for the *halide interactions* $|Q_x|$ has in all cases the largest value. The Q_x axis is located in the same octant as the A_x axis and is also pointing approximately in the direction of the nearest S (or Se) p_y lobe of the X_2^- ion (monovacancy model).

The Q tensor contribution from the charge distribution of the unpaired electron on the nucleus can be derived using Eq. (3). This contribution is proportional to A^c [Eq. (3)] with the following proportionality constant C:

$$C = \frac{-e^2 Q}{2I(2I-1)} \frac{1}{4\pi\epsilon_0} \left(\frac{\mu_0}{4\pi h}\, g_N g_e \beta \beta_N 10^{-6} \right)^{-1}, \tag{10}$$

in which Q is the quadrupole moment. The resulting axial Q tensors are denoted in Table XII. For the axis corresponding

with the largest Q value, the angles with respect to the g tensor axes are given.

When comparing Table XII with Tables III and IV, we remark that although the axes of the largest Q value are located in the same octant, no quantitive match was found. The found discrepancy might be explained by taking into account the spatial distribution of the charges over the p lobes of the surrounding ions.

The observed Q tensors for the *sodium interactions* can be explained in a similar way. From the derivation of the A tensor for interaction 2 it was found that the wave function of the unpaired electron in the neighborhood of the Na nucleus is given by Eq. (5). The corresponding contribution to the Q tensor is proportional to A^c [Eq. (6)] with proportional constant C.

The contribution of the surrounding ions to the Q tensor can be calculated in the following way. The resulting field gradient due to the six nearest-neighboring anions surrounding the cation is calculated. Therefore, the displacements of the Na atoms with respect to the X_2^- defect, obtained from the SHF tensor analysis, are taken into account, whereas the surrounding halide ions are assumed to be on their normal lattice positions. This will probably not be the case in practice, which may alter the result. The distribution of the unpaired electron over the X_2^- orbitals and the distribution of the negative charge over the three valence p orbitals of the halide ions are also considered. The obtained values have to be multiplied with $eQ/(2I(2I-1))$ and $(1-\gamma_\infty)$ to obtain the contribution to the Q tensor in MHz. γ_∞ is the Sternheimer shielding factor.[33]

Combination of the two contributions leads for interaction 2 to

$$\mathrm{NaBr{:}S_2^-}: Q_x = 0.022 \ \mathrm{MHz}, \quad Q_y = -0.040 \ \mathrm{MHz},$$

$$Q_z = 0.018 \ \mathrm{MHz},$$

$$\mathrm{NaI{:}S_2^-}: Q_x = 0.034 \ \mathrm{MHz}, \quad Q_y = -0.086 \ \mathrm{MHz},$$

$$Q_z = 0.052 \ \mathrm{MHz}.$$

These results are in nice agreement with the observed Q tensors (Table VI).

Comparison between Tables V and VI shows that the principal values of interaction 1 are a factor 3–10 larger than the ones observed for interaction 2. To calculate the Q tensor, again two contributions have to be taken into account.

The wave function of the unpaired electron in the neighborhood of the alkali-metal ion A [Fig. 4(a)] is given by Eq. (8). The resulting Q components are again proportional to the resulting SHF matrix with the proportional constant C. Although the c_π^2 values mentioned in Table X are not exact, they are sufficient as a measure for the contribution of the unpaired electron in the p_y orbital. The resulting Q tensors are axial around the y axis with Q_y ($\mathrm{NaBr{:}S_2^-}$) $=-0.022$ MHz, Q_y ($\mathrm{NaI{:}S_2^-}$) $=-0.019$ MHz, and Q_y ($\mathrm{NaBr{:}Se_2^-}$) $=-0.032$ MHz. The influence of the surrounding ions on the Q tensor also has to be taken into account. When assuming the Na^+ ions to be located on a lattice site, the largest Q value does not exceed 0.10 MHz, what is clearly less than the observed values. This suggests that the Na^+ ions A [Fig. 4(a)] have to be displaced with respect to their lattice positions. The same conclusion was drawn from the investigation of the SHF matrix.

IV. CONCLUSION

The single-crystal ENDOR spectra of $\mathrm{NaBr{:}S_2^-}$, $\mathrm{NaBr{:}Se_2^-}$, and $\mathrm{NaI{:}S_2^-}$ allowed a detailed analysis of the interactions with the surrounding sodium and halide ions. The orientations and principal values of the A and Q tensors were determined.

The observed halide interactions could be ascribed to eight equivalent next-nearest-neighboring halide ions. One sodium interaction is caused by the nearest-neighboring Na ions in the (001) plane. The alkali ions responsible for the second sodium interaction are the two nearest-neighboring cations along the [001] axis. Information about the wave functions of the unpaired electron in the neighborhood of the observed halide and sodium nuclei could be derived. The only model consistent with these ENDOR data is that of the X_2^- (X=O,S,Se) molecular ion substituting for a single halide ion on a lattice site. The nearest-neighboring Na^+ ions are found to be outwards displaced. The observed EPR linewidths could be explained in terms of this monovacancy and the observed SHF interactions.

ACKNOWLEDGMENTS

This work is part of a project sponsored by ''Interuniversitair Instituut voor Kernwetenschappen'' (IIKW), Belgium. S. Van Doorslaer and F. Callens wish to thank the NFSR, Belgium, for financial support.

[1] W. Känzig and M. H. Cohen, Phys. Rev. Lett. **3**, 509 (1959).
[2] H. R. Zeller and W. Känzig, Helv. Phys. Acta **40**, 845 (1967).
[3] R. T. Shuey and H. R. Zeller, Helv. Phys. Acta **40**, 873 (1967).
[4] L. E. Vannotti and J. R. Morton, Phys. Rev. **161**, 282 (1967).
[5] L. E. Vannotti and J. R. Morton, Phys. Lett. **24A**, 250 (1967).
[6] P. Matthys, F. Callens, and E. Boesman, Solid State Commun. **45**, 1 (1983).
[7] R. Callens, F. Callens, P. Matthys, and E. Boesman, Phys. Status Solidi B **148**, 683 (1988).
[8] F. Callens, F. Maes, P. Matthys, and E. Boesman, J. Phys. Condens. Matter **1**, 6912 (1989).
[9] F. Maes, F. Callens, P. Matthys, and E. Boesman, J. Phys. Chem. Solids **51**, 1289 (1990).
[10] F. Maes, F. Callens, P. Matthys, and E. Boesman, Phys. Status Solidi B **161**, K1 (1990).
[11] F. Maes, P. Matthys, F. Callens, and E. Boesman, Solid State Commun. **80**, 583 (1991).
[12] F. Maes, P. Matthys, F. Callens, P. Moens, and E. Boesman, J. Phys. Condens. Matter **4**, 249 (1992).
[13] H. Fabian and F. Fischer, J. Lumin. **43**, 103 (1989).
[14] H. Fabian and F. Fischer, J. Raman Spectrosc. **20**, 639 (1989).

[15] S. Van Doorslaer, F. Callens, F. Maes, and E. Boesman, Phys. Rev. B **51**, 12 480 (1995).
[16] S. Van Doorslaer, F. Callens, F. Maes, and P. Matthys, J. Phys. Condens. Matter **7**, 1909 (1995).
[17] S. Van Doorslaer, F. Maes, F. Callens, P. Moens, and E. Boesman, J. Chem. Soc. Faraday Trans. **90**, 2541 (1994).
[18] S. Van Doorslaer, F. Callens, F. Maes, and P. Matthys, J. Phys. Condens. Matter **7**, 9279 (1995).
[19] R. Gazzinelli and R. L. Mieher, Phys. Rev. **175**, 395 (1968).
[20] M. L. Dakss and R. L. Mieher, Phys. Rev. Lett. **18**, 1056 (1967).
[21] M. L. Dakss and R. L. Mieher, Phys. Rev. **187**, 1053 (1969).
[22] D. F. Daly and R. L. Mieher, Phys. Rev. **183**, 368 (1969).
[23] *Tables of Interatomic Distances and Configurations in Molecules and Ions*, edited by L. E. Sutton (Chemical Society, London, 1958), p. M69.
[24] G. F. Koster, J. O. Dimack, R. G. Wheeler, and H. Satz, *Properties of the Thirty-Two Point Groups* (MIT Press, Cambridge, MA, 1963).
[25] A. K. Koh and D. J. Miller, At. Data Nucl. Data Tables **33**, 235 (1985).
[26] G. C. Hurst, T. A. Henderson, and R. W. Kreilick, J. Am. Chem. Soc. **107**, 7294 (1985).
[27] G. E. Holmberg, W. P. Unruh, and R. J. Friauf, Phys. Rev. B **13**, 983 (1976).
[28] M. T. Barriuso and M. Moreno, Phys. Rev. B **26**, 2271 (1982).
[29] M. Bucher, J. Phys. Chem. Solids **54**, 301 (1993).
[30] M. Iwasaki, J. Magn. Reson. **16**, 417 (1974).
[31] N. M. Atherton, *Principles of Electron Spin Resonance* (Ellis Horwood, London, 1993).
[32] J. D. Graybeal, *Molecular Spectroscopy* (McGraw-Hill, New York, 1988).
[33] R. M. Sternheimer, Phys. Rev. **146**, 470 (1966).